Open access • Posted Content • DOI:10.1007/S13538-021-01016-0

Graphene-Based Tunable Broadband Polarizer for Infrared Frequency

Vishal Sorathiya, Shobhit K. Patel

Institutions: Marwadi University

Published on: 01 Feb 2022 - Brazilian Journal of Physics (Springer US)

Topics: Polarizer, Circular polarization, Polarization (waves), Graphene and Terahertz radiation

Graphene-based tunable broadband polarizer for infrared frequency

Vishal Sorathiya (vishal.sorathiya9@gmail.com)
Marwadi Education Foundation's Group of Institutions https://orcid.org/0000-0002-6121-5940
Shobhit K Patel
Marwadi University

Research Article

Keywords: Polarizer, Tunability, Infrared, Metasurface, Graphene

Posted Date: August 13th, 2021

DOI: https://doi.org/10.21203/rs.3.rs-808726/v1

Version of Record: A version of this preprint was published at Brazilian Journal of Physics on November 16th, 2021. See the published version at https://doi.org/10.1007/s13538-021-01016-0.

Graphene-based tunable broadband polarizer for infrared frequency

Vishal Sorathiya[1,3,#], Shobhit K Patel[2]
[1]Department of Information and Communication Technology, Marwadi University, Gujarat, Rajkot, 360003 India
[2]Department of Computer Engineering, Marwadi University, Gujarat, Rajkot, 360003 India
[3]Department of Electronics and Communication, Marwadi University, Gujarat, Rajkot, 360003 India
[#]Corresponding Author: vishal.sorathiya@marwadieducation.edu.in, Tel: +919033316057

Abstract

This paper proposes the tunable graphene-assisted polarizer structure which is working on the infrared frequency range. The tunable polarizer has been designed by a three-layered structure of silica, graphene, and gold. The polarizer behavior of the structure is analyzed for the frequency range of 3 to 12 THz. The tunability of the structure is analyzed for the different values of fermi energy which is tunable parameter of single-layer graphene sheet. Polarizer response is derived in terms of different performance parameters such as reflectance, phase variation, phase difference, polarization conversion rate, and effective refractive indices. Graphene-based polarizer structure is investigated for the co-polarization and cross-polarization input incident conditions to check linear to circular polarization conversion. It also shows an effective refractive index response to check the metasurface behavior of the polarizer for 3 to 12 THz range. We have observed that the polarization amplitude becomes stronger for the higher Fermi energy value of the graphene sheet. The reflection amplitude is achieved up to 90%. Results of the proposed polarizer structure can be used to design the various electro-optical structure which operates in the lower THz range.

Index Terms

Polarizer, Tunability, Infrared, Metasurface, Graphene

1. INTRODUCTION

Metamaterials are materials that are arterially fabricated. Graphene is very popular due to its small scale, low costs, and ultrathin thickness[1]. The metamaterial can be engineered to obtain the interesting properties that natural materials do not possess, such as ideal lens, hyperbolic dispersion, negative refractive index, etc[2]–[5]. Graphene consists of six carbon atoms and a single atomic thick structure. Due to its high thermal, electrical, and optical properties, graphene is very popular[6]. Graphene is also commonly used in the construction of many reconfigurable devices such as gratings [7], tunable absorbers [8], [9], polarizers [2], leaky-wave antennas[10], etc. It can be reconfigured by adjusting different physical characteristics such as

chemical potential, temperature, frequency, and dispersion rate [11]. The intra-band conductivity model of graphene can be investigated by the Dirac cone[12]. It has been analyzed that graphene provides the control action by an external magnetic field or electrostatic [13] that varies from one material to another. Also, a high electrical/optical conductivity can be observed with the adaptation of graphene from the near-infrared spectrum [14] to the far-infrared region[15]. The conception of graphene-based photonics systems is based on creating integrated geometry using single-layered sheets. The principle of constructing metamaterial (MM) and graphene polarisation structures can be explored by taking into consideration the various geometries of the graphene sheet [16], [17]. Polarizers are structures that can be used as electromagnetic filters for the development of periodically directed structures [18]. They can be used as electromagnetic equipment for different types of applications that may include as radiographic antennas, metamaterial, stealth systems, reduction in radar cross-sections, etc [19]. Using THz absorption graphene material and a polarizer, several research studies have been performed on the selective surface-based structure as mentioned in [20], [21]. The graphene-based polarizers can mainly be tuned with the help of chemical graphene potentials and the frequency which can be altered and can be modified externally[22].

In this manuscript, we have presented the graphene-based broadband metasurface polarizer structure which is working for the far-infrared frequency spectrum. The proposed metasurface polarizer is analyzed for different physical parameters such as reflectance coefficient, co polarization, cross-polarization, Polarization conversion rate (PCR), and wide-angle incident values. In the first section of the manuscript, the design of the polarizer is presented. The second section of the manuscript shows the mathematical model of graphene. Discussion of the different physical parameters and results derived from the designed polarizer is shown in the last section of the manuscript.

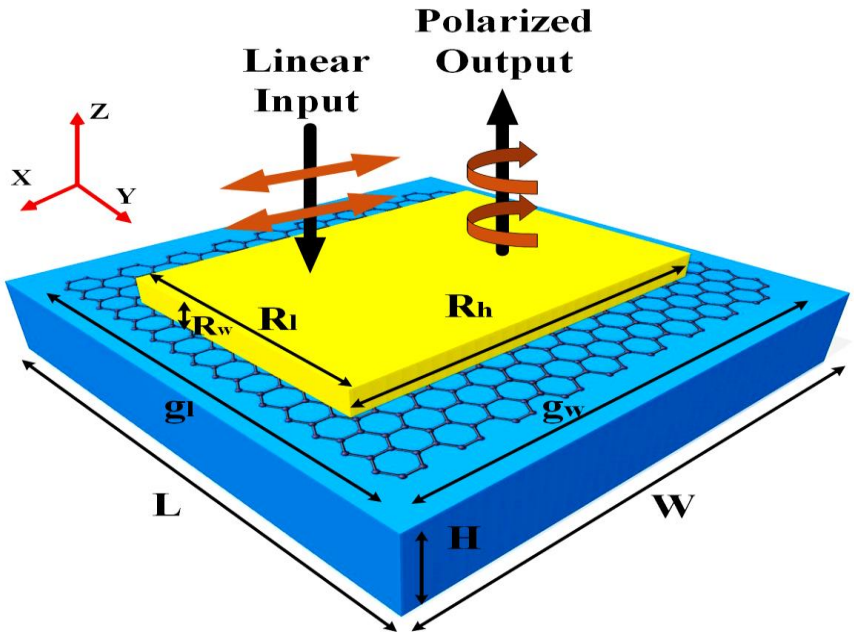

Fig 1: Schematic of broadband polarizer using graphene-based structure for far-infrared frequency spectrum. Different dimensions of the structures are define as: H = 1.5 µm, W = 7.6 µm, L = 7.6 µm, g_l = 3 µm, g_w = 4 µm, R_w= 0.2 µm, R_h = 6.5 µm and R_l=5 µm. Polarized input wave is excited from the Z – direction

2. Polarizer design and graphene conductivity model

2.1 Graphene-based broadband polarizer design

The 3D (three-dimensional) view of the graphene-based tunable broadband polarizer is shown in Fig. 1.The single-layer graphene sheet is placed over the silica material slab and on top of it, a rectangular gold slab is placed as illustrated in Fig. 1. The different dimensions of the structure can be define as follows: H = 1.5 µm, W = 7.6 µm, L = 7.6 µm, gl = 3 µm, gw = 4 µm, Rw= 0.2 µm, Rh = 6.5 µm and Rl=5 µm. The input incident wave of range 3 to 12 THz is excited from the Z – direction. The proposed structure is designed by considering periodic boundary conditions over the X and Y directions. The structure is excited by the different polarized conditions (X and Y -polarized) from the top of the structure.

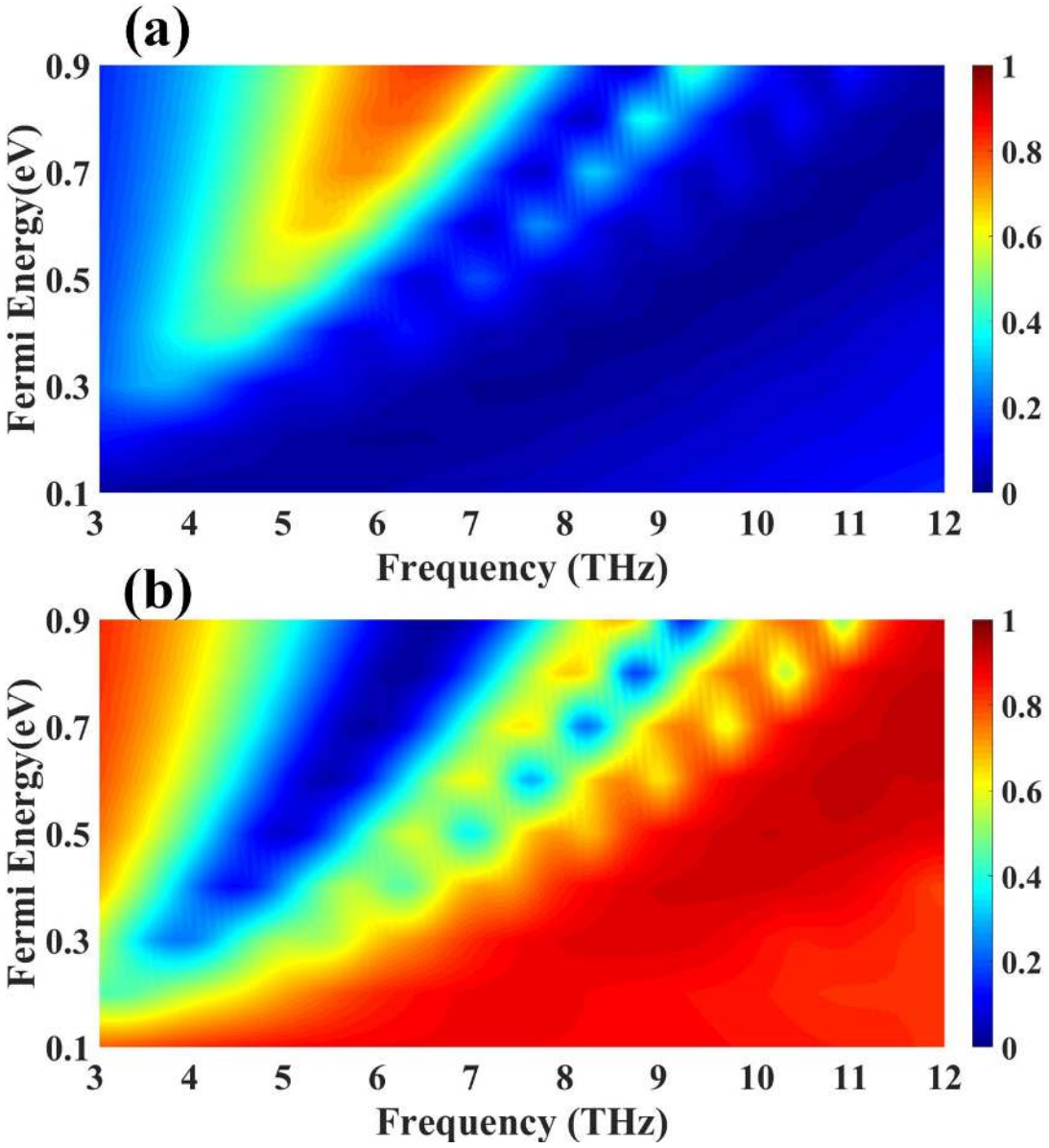

Fig 2: (a) Reflection and (b) transmittance response of the polarizer structure for X – polarized incident wave. Responses are derived for the infrared range of 3 to 12 THz and different values of Fermi energy of the graphene sheet.

2.2 Graphene conductivity model and possible fabrication methods

The single sheet of graphene can be articulated as a conductivity model using the Kubo formula [13]. The proposed polarizer structure is investigated using the finite element method (FEM). The proposed structure is investigated using a graphene surface conductivity model which can be implemented by the formula given in Eq. (1-4). The graphene conductivity model can be presented by intramodal and intermodal conductivity equations as shown in Eq. 2-4.

$$\varepsilon(\omega) = 1 + \frac{\sigma_s}{\varepsilon_0 \omega \Delta} \tag{1}$$

$$\sigma_{intra} = \frac{-je^2 k_B T}{\pi\hbar^2(\omega - j2\Gamma)}\left(\frac{E_f}{k_B T} + 2\,ln\left(e^{-\frac{E_f}{k_B T}} + 1\right)\right) \tag{2}$$

$$\sigma_{inter} = \frac{-je^2}{4\pi\hbar} ln\left(\frac{2|E_f| - (\omega - j2\Gamma)\hbar}{2|E_f| + (\omega - j2\Gamma)\hbar}\right) \tag{3}$$

$$\sigma_s = \sigma_{inter} + \sigma_{intra} \tag{4}$$

The specifications & values of the parameters which are presented in the above equation have been described in Table 1. The graphene Fermi potential as a function of the gate bias voltage can be defined as $E_f = \hbar v_F \sqrt{\pi C V_{bg}}$. where $C = \varepsilon_0 \varepsilon_d / H$ is Electro statistic capacitance per unit area. The parameters like - ε_0 is defined as permittivity of free space, ε_d (2.25) defined as permittivity of silica material and H (1.5 µm) describes the thickness of the silica layer. The graphene conductivity equation will result in complex values. This equation also affects the resistive and reactive behaviour of the system. From the calculation of the graphene sheet in FEM simulation, the surface current destiny values such as $J_x = E_x\sigma_s \; and \; J_y = E_y\sigma_s$ have been assigned to the graphene surface in the X and Y direction. The tetrahedral Delaunay tessellation meshing condition has been chosen for the proposed polarizer structure. The maximum and minimum size of the meshing is set as 150 nm and 15 nm respectively. The growth rate value of meshing is set to 0.6. The most common methods used for creating two-dimensional material and single-layer graphene are Cleavage techniques [23] as well as CVD [24] and MBE [25] techniques. The wet and dry transition structures, for example, plasmonics structure lithography [26], atomic force nanolithography [27], nano spheric lithographic process [28], and so on, are also transferable by many methods. A complicated structure on the top layer of the graphene material can be fabricated via nano-spheric lithography [28] and lithography of nanoplasmonics devices [26]. As seen in [26], where lithography technologies for plasmonics device fabrication process have been applied, resulting in graphene composite with high quality and versatile complex nano and microstructures. The transfer process of gold structure on the graphene layer can be realized by the process of transfer printing of graphene using gold film [27]. The experimental method for creating the pattern-based gold surface is shown in [27]. The proposed structure can also be fabricate using CVD and electron beam lithography method as suggested in [28].

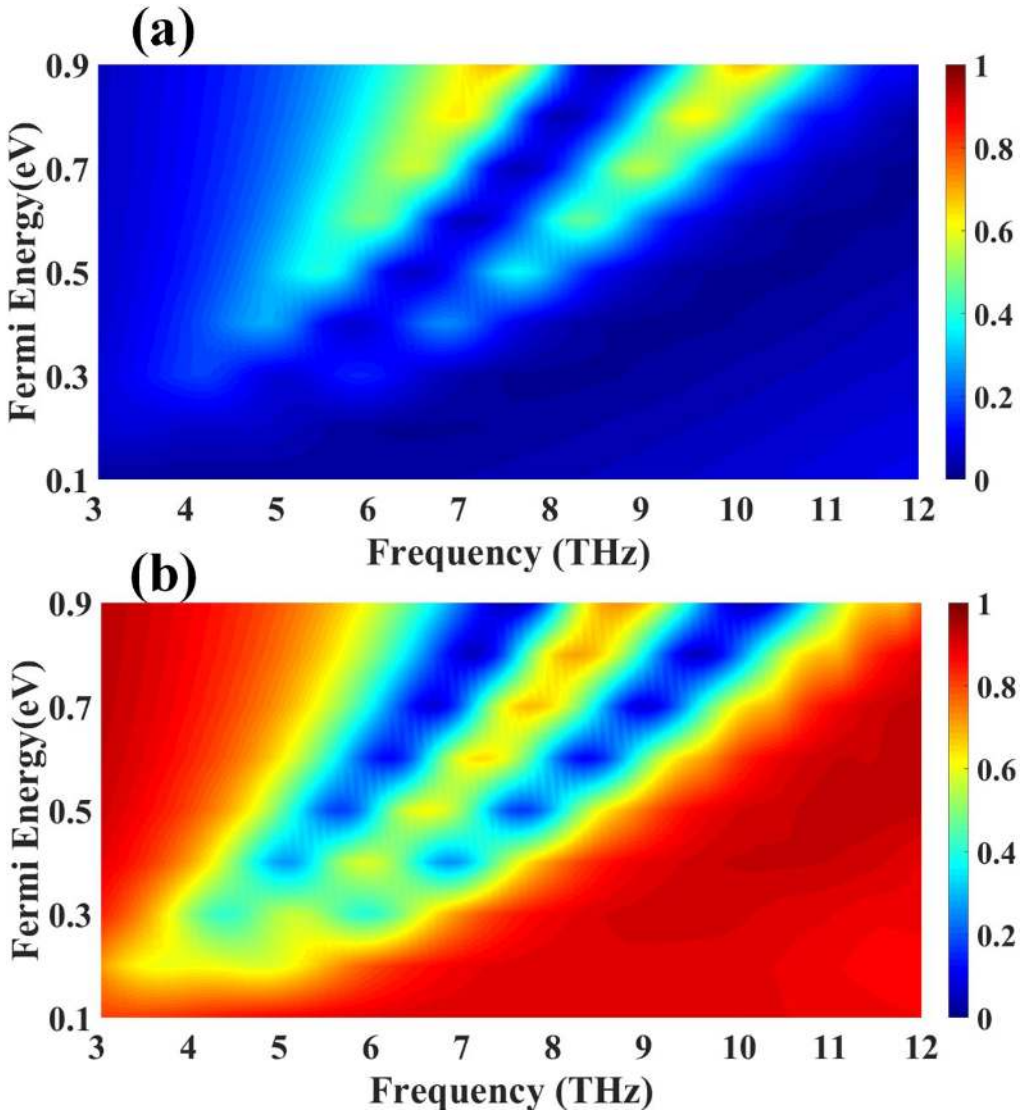

Fig 3: (a) Reflection and (b) transmittance response of the polarizer structure for Y – polarized incident wave. Responses are derived for the infrared range of 3 to 12 THz and different values of Fermi energy of the graphene sheet

TABLE I

Parameter specification and values of Eq. (1-4)

Parameters	Specification	Values
ω	Radian frequency	3 THz to 12 THz
Γ	Scattering rate	10^{-11}
ħ	Reduced plank constant	$6.582119569 \times 10^{-16}$ eV.s
kB	Boltzmann constant	$8.617333262 145 \times 10^{-5}$ eV.K^{-1}

E_f	Fermi energy	0.1 eV to 0.9 eV
τ-1	Electron relaxation time	10^{-13} s
T	Temperature	300K

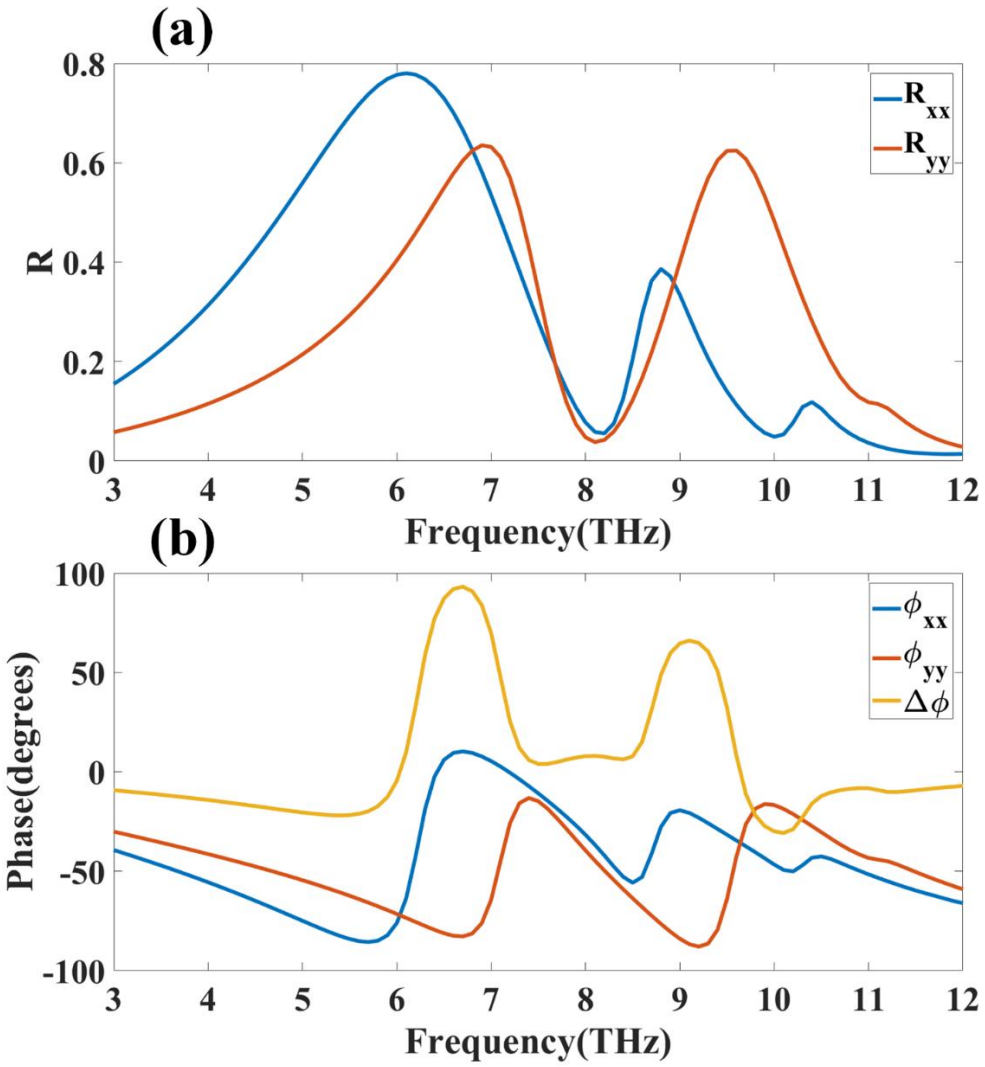

Fig 4: (a) Reflectance coefficient response and (b) Phase difference response for X- polarized and Y – polarized incident waves.

2.3 Tunability response and refractive coefficient value

Mathematical modeling of graphene gives an idea to control conductivity using external parameters. In general, graphene conductivity value can be controlled with the help of various parameters such as temperature, Fermi energy, frequency, and scattering rate. The tunability behavior of the proposed broadband polarizer structure is numerically investigated by applying different Fermi energy. The reflectance and transmittance response of the proposed structure is shown in Fig. 1 and Fig. 2 for different modes of polarization. Fig. 2(a) shows the reflectance response for the X – polarization structure. Similarly, the

transmittance response for the X- polarizer wave is shown in Fig. 2(b). Tunable behavior of the structure is derived for a range of 3 to 12 THz. The graphene Fermi potential is varied between 0.1 - 0.9 eV. Fig. 3(a) and Fig. 3(b) show the reflectance coefficient and transmittance coefficient response for the Y – Polarized wave. The reflectance coefficient is defined as $R_{ij} = \left|E_j^{Reflec}/E_i^{Inc}\right|(i,j = x,y)$, where $E_j^{Reflec}(j = x,y)$ is the x or y component of the reflected wave and $E_j^{Inc}(j = x,y)$ is the x or y component of the incident wave [29].

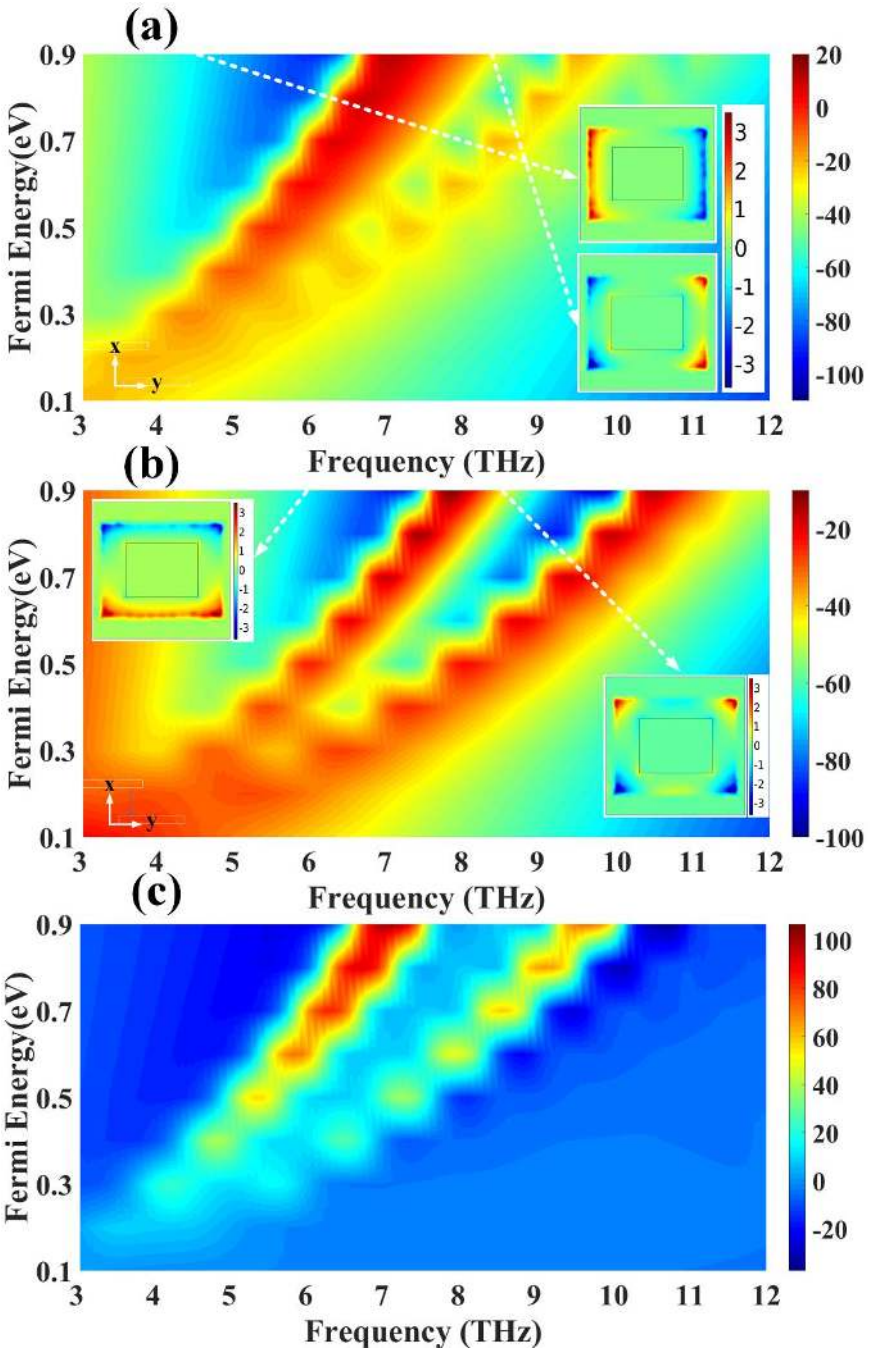

Fig 5: Calculated phase difference response and phase variation response for the input function of frequency and Fermi energy of the graphene sheet. Phase variation for (a) X – Polarized wave (Φ_{xx}) and (b) Y – Polarized wave (Φ_{yy}). Inset: z – components of the electric field intensity for different resonating points. (c) phase difference for both polarized waves ($\Delta\Phi$).

Variation in R_{xx} and R_{yy} amplitudes are due to the dipole moment created for different input incident wave conditions. Overall covered area of rectangular gold and graphene shape of the graphene patch is considered as rectengular with $R_l \neq R_h \; and \; g_l \neq g_w$ condition. A significantly bigger difference in wavelength shift is achieved by making a larger difference between the length-width of the graphene and gold structure. The resonating frequency of the graphene depends on the length and width of the structure by considering the function $f_r \; \alpha \sqrt{E_f/L}$ [30]. Where, $E_f = \mu_c = Fermi \; energy$ of the graphene sheet. The resonance at selective frequency will generate by the creation of dipole moment over graphene and gold sheet as shown in the inset of Fig. 5 (a) and Fig. 5(b). From the above response, we have calculated that the different geometries of graphene and gold structure can create different resonance points at different resonating frequencies.

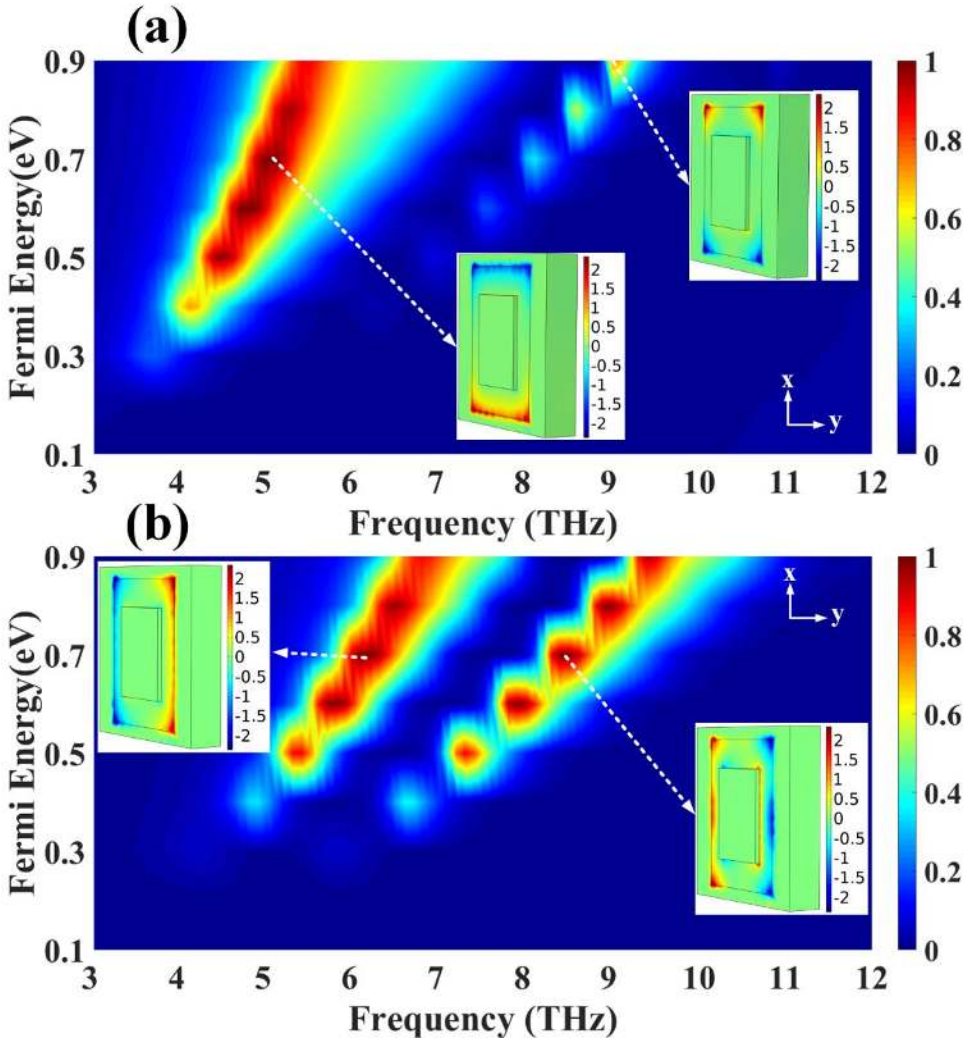

Fig 6: Calculated PCR response of the different cross-polarization graphene-based polarizers as the function of Fermi energy and incident frequency. (a) PCR response for X-Y cross-polarization and (b) Y-X cross-polarization. Inset: Electric field intensity E_z values for the different resonating points

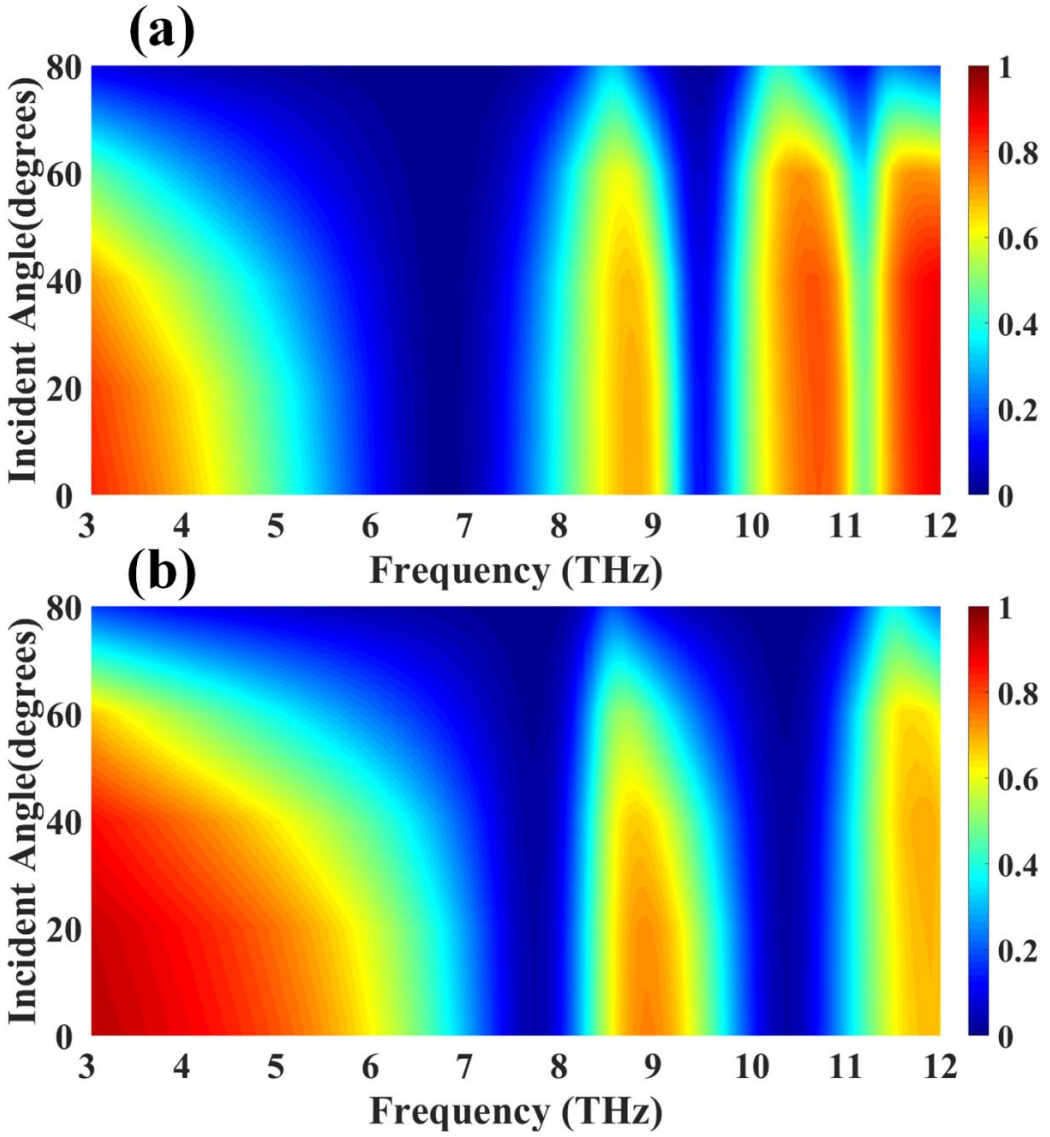

Fig 7: Calculated reflectance response as a function of the wide incident angle of the input wave. (a) Wide-angle response for the X – polarized incident wave. (b) wide-angle response for Y – polarized wave. The Fermi energy of the calculated response is chosen as 0.9 eV.

2.4 Phase variation and polarization conversion rate

The phase is defined as $\Phi_{ij} = \arg\left(E_j^{Reflec}/E_i^{Inc}\right)(i,j = x,y)$. The phase difference between the incident and the reflected wave is presented as $\Delta\Phi = \Phi_{xx} - \Phi_{yy}$. Comparative response of reflectance coefficient (co-polarized) for both incident polarized waves are presented in Fig. 4(a). The phase difference for both polarized waves is shown in Fig. 4(b). We have observed about -80° to 10° of polarization variations for the X – polarized incident wave condition. Similarly, we have observed -80° to -10° of the polarization variation for the Y -polarized incident wave condition. A rise in the reflectance for the same range of the polarization variation can be observed in Fig. 4(a). The phase difference between both of these waves is observed to be more than 90°. Overall, it is found that the phase difference of 90° has been distinguished over the range of 6 to 7 THz with higher values of reflectance amplitude. Similarly, 60° of the phase differences have been observed in the range of 8.8 to 9.5 THz. The variation in the phase difference for the different values of

frequency and applied graphene Fermi potential is shown in Fig. 5. Fig.5(a) shows the variation in the phase for X – polarized wave. Similarly, Phase variation for the Y-polarized incident wave condition is shown in Fig. 5(b). Inset images of each figure show the variation in the electric field intensity E_z for different resonating points. A 90° phase variation in E_z response for two of the resonating points can be observed. The maximum variation of the phase difference is observed in the range of -100° to 20° for the X – polarized incident wave.

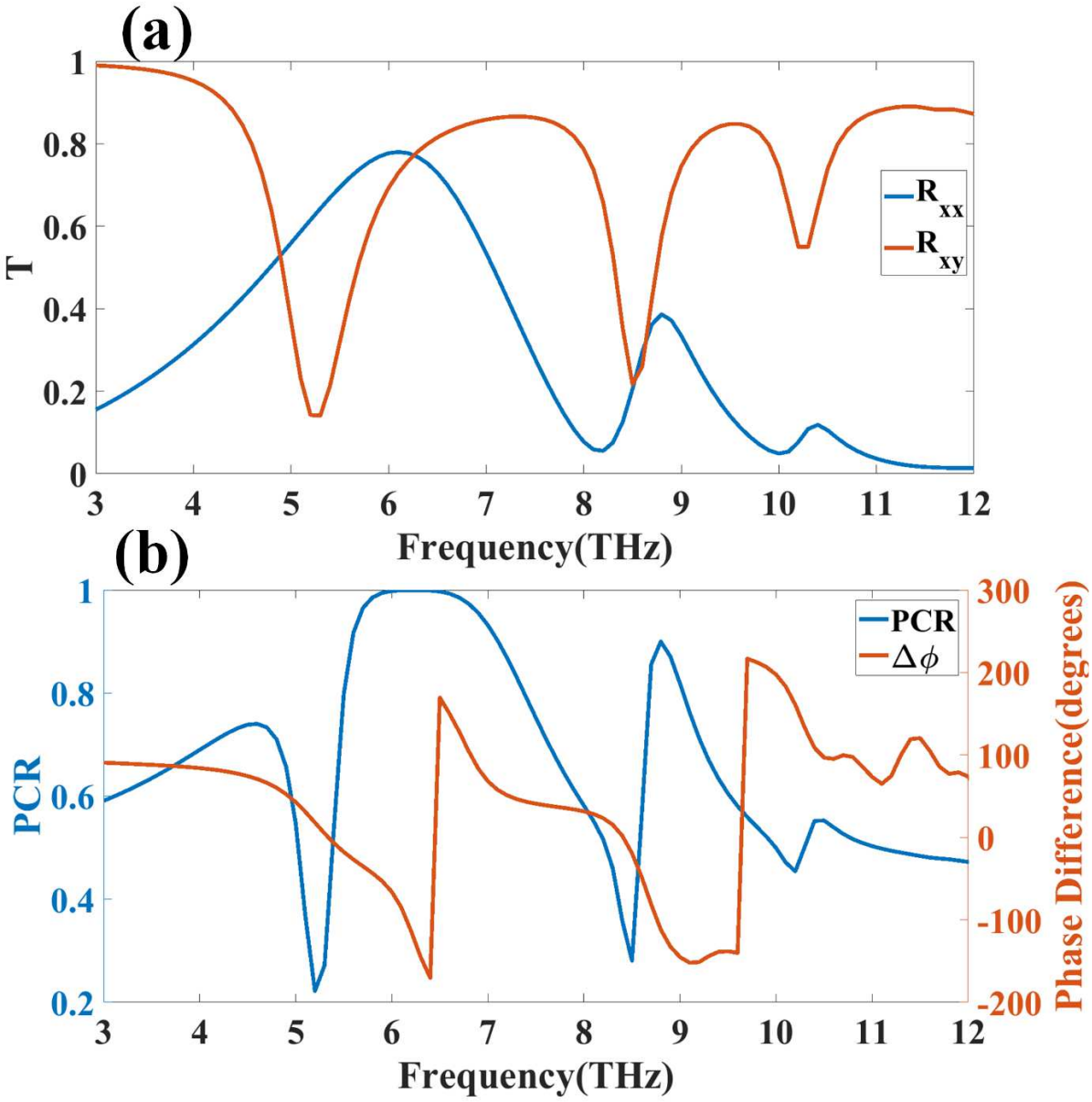

Fig 8: (a) Reflection coefficient for the co-polarization (R_{xx}) and cross-polarization (R_{xy}) for input wave condition as X – polarized, (b) PCR and phase difference response.

Similarly, In Y – polarized incident wave, phase variation is observed to be in the range of -100° to -10°. A phase difference between X and Y polarized waves is shown in Fig. 5(c). The phase differences of about -20° to 100° in both incident waves can be observed. The elliptical polarization of the input incident wave will be generated when $R_{xx} \neq R_{yy}$ and $\Delta\Phi = 90°$ conditions satisfy. Similarly, circular polarization of the

input incident wave can be generated when $R_{xx} = R_{yy}$ and $\Delta\Phi = 90°$ conditions satisfy. We can observe such conditions in Fig. 4 (a) and Fig. 4(c).

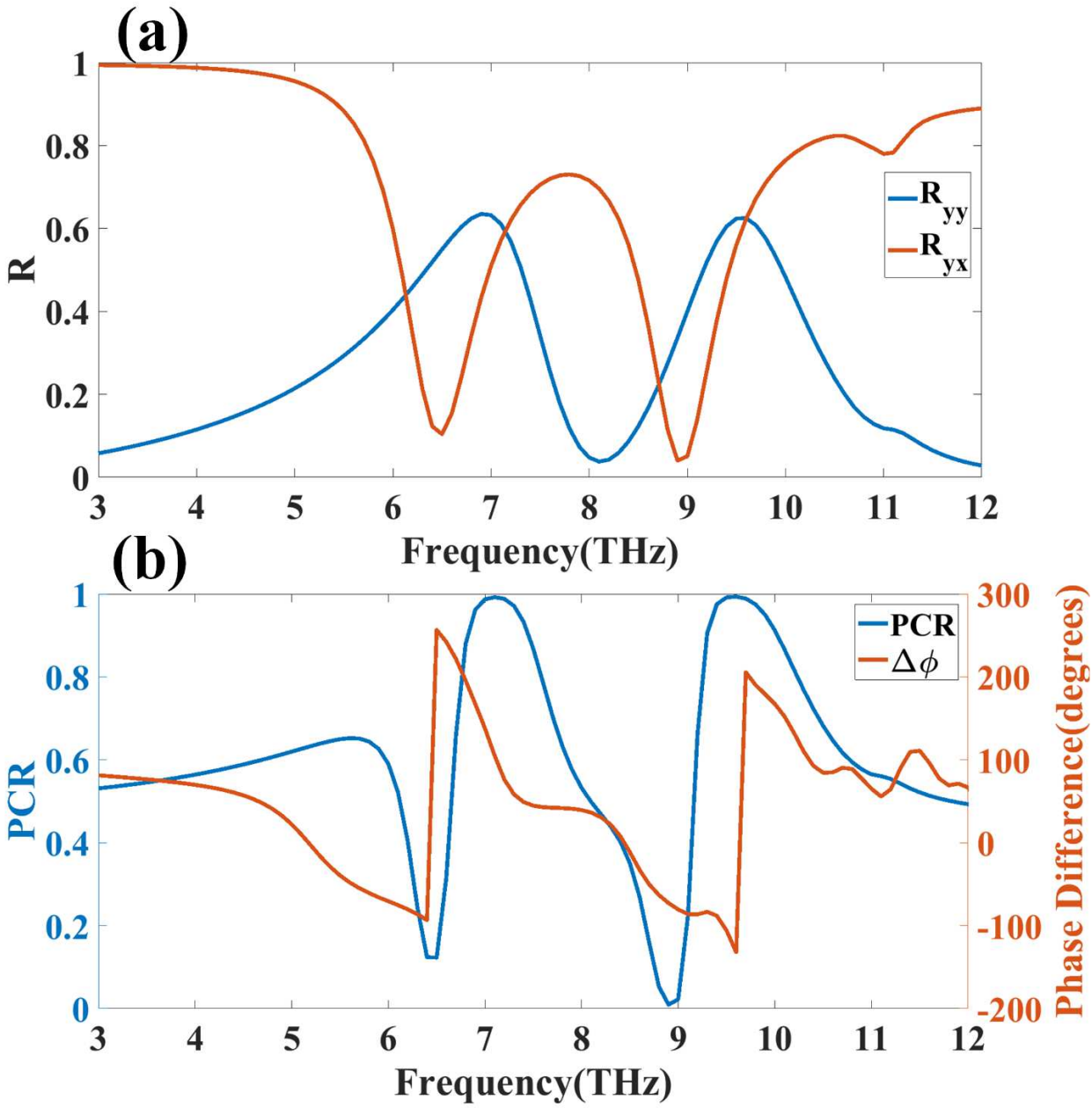

Fig 9: (a) Reflection coefficient for the co-polarization (R_{yy}) and cross-polarization (R_{yx}) for input wave condition as Y – polarized,(b) PCR and phase difference response.

This behavior proves the working of the proposed structure as linear to the elliptical and linear to the circular polarizer. The polarization conversion rate is defined as $PCR = |R_{xy}|^2 / \left[|R_{xx}|^2 + |R_{xy}|^2\right]$ [31] to reveal the performance of the proposed polarizer as a behavior of cross-polarization. The PCR for the X-Y cross-polarization and Y- X cross-polarization have been shown in Fig. 6(a) and Fig. 6(b) respectively. Inset figures are showing the E_z components of the different resonating points for both cross-polarization effects. Values of PCR are observed more than 90% in both of the cases. Tunable behavior of PCR can be achieved by applying different frequencies and Fermi energy. It is also observed that for the higher chemical potential the

value of PCR is more than 80% for the different resonating bands. Reflectance behavior for the wide-angle incident response is investigated for the range of 0° to 80° of the incident angles. The reflectance coefficient variation for the wide-angle incident is presented in Fig. 7 for the X and Y polarized incident wave. Constant reflectance below the 4 THz frequency has been observed for X – polarized incident wave condition. It is also observed (Fig. 7(a)) that for X – polarized wave, a constant reflectance response below the 60° for a higher frequency range (>8 THz) Similarly, it is observed constant reflectance response for below the 60° of incident angle on 3 THz to 6 THz range. The wide-angle incident graph is derived by applying the 0.9 eV to the graphene sheet.

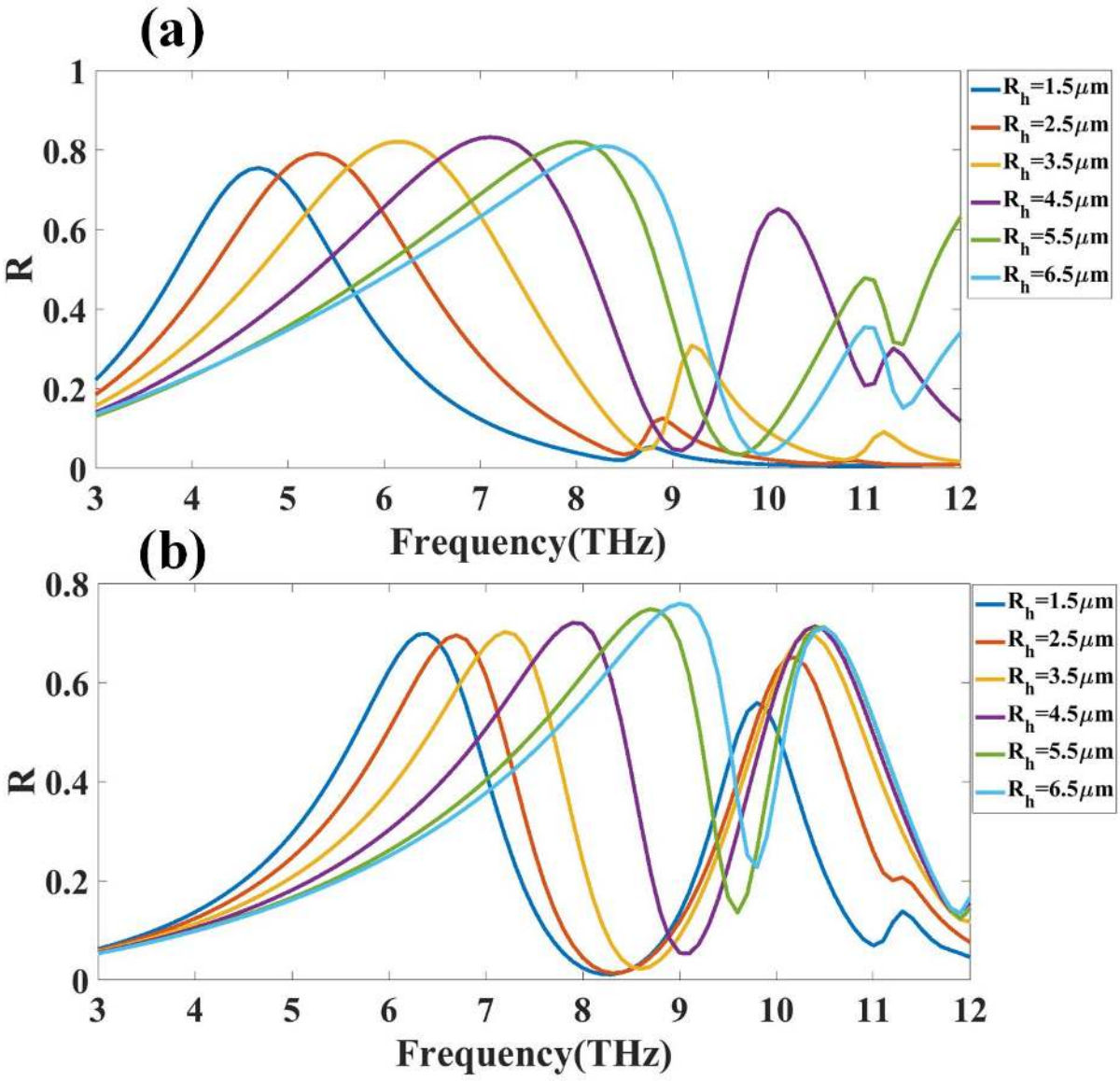

Fig 10: Calculated reflectance coefficient values for (a) X and (b) Y – polarized incident wave conditions as a function of frequency and R_h

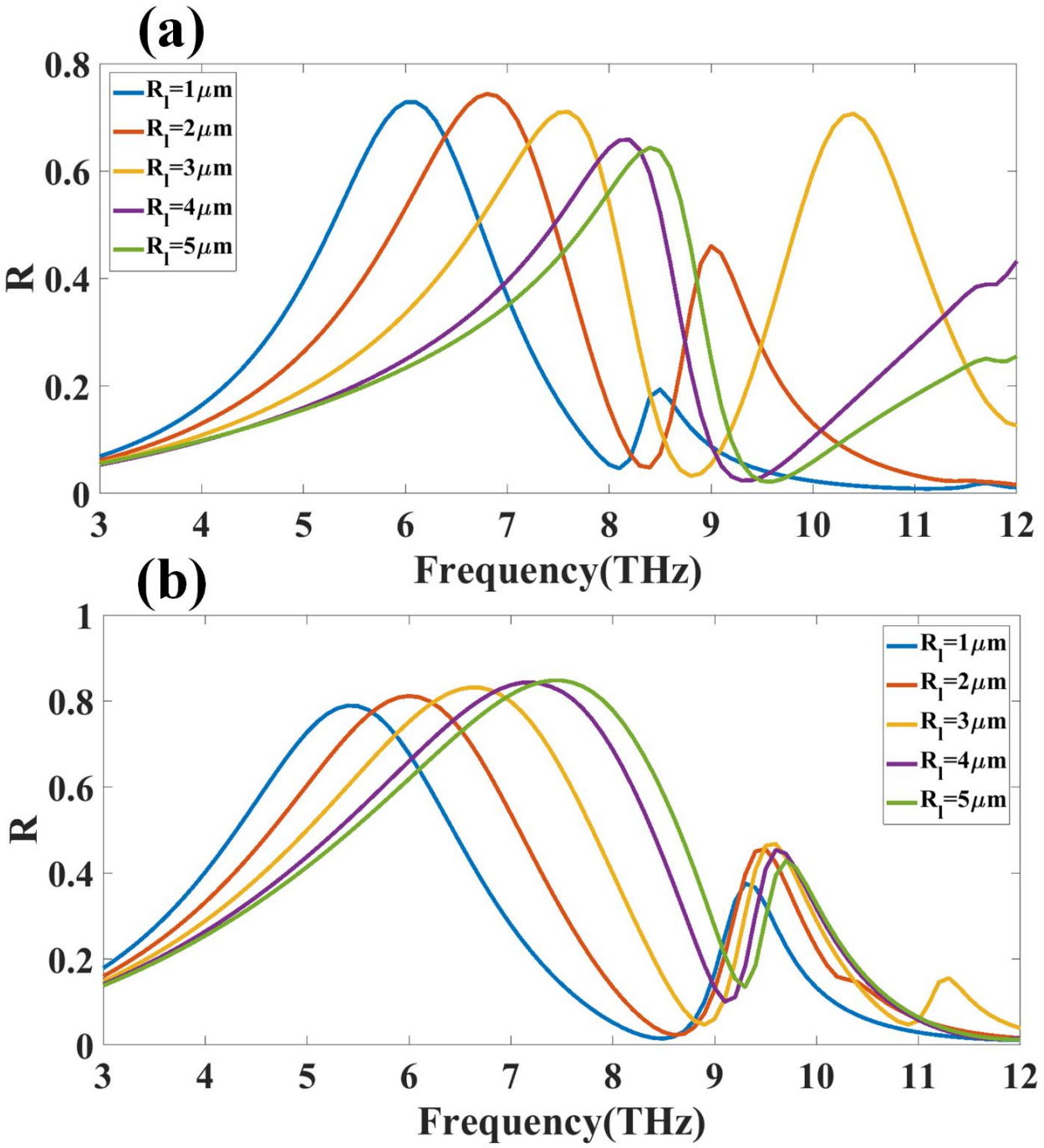

Fig 11: Calculated reflectance coefficient values for (a) X and (b) Y – polarized incident wave conditions as a function of frequency and R_l

2.5 Cross polarization behavior and effect of physical parameters

The combined response of the reflection coefficient for the co-polarized and cross-polarized wave is shown in Fig. 8(a) and Fig. 8(b). Fig. 8(a) shows the co-polarization R_{xx} and cross-polarization R_{xy} for the X – polarized wave conditions. Similarly, Fig. 8(b) shows the co polarization R_{yy} and cross-polarization R_{yx} for the Y-polarized incident wave conditions. PCR and the phase difference response between co and cross-polarization have been illustrated in Fig. 9(a) and Fig. 9(b) for X and Y polarization incident wave conditions.

The effect in reflectance amplitude for different values of physical parameters is presented in Fig. 10 and Fig. 11. Fig. 10 shows a variation in reflectance amplitude as a function of frequency and R_h. Fig. 10 (a) and Fig. 10(b) shows the variation in reflectance for X polarized and Y polarized wave. It is observed that the large frequency shift over the 3 THz to 12 THz range of different values of R_h. R_h is varied from 1.5 µm to 6.5 µm. Fig. 11 shows a variation in reflectance as a function of frequency and R_l. Fig. 11(a) and Fig. 11(b) show the variation in reflectance for the X polarized and Y polarized wave respectively for the different values of R_l. A large frequency shift of about 3 THz to 12 THz range for different values of R_l can be remarked. Values of R_l are varied from 1 µm to 5 µm. From the response of the parameter changes & reflectance amplitude – we can conclude that the performance of the polarizer can be controlled from various physical parameters.

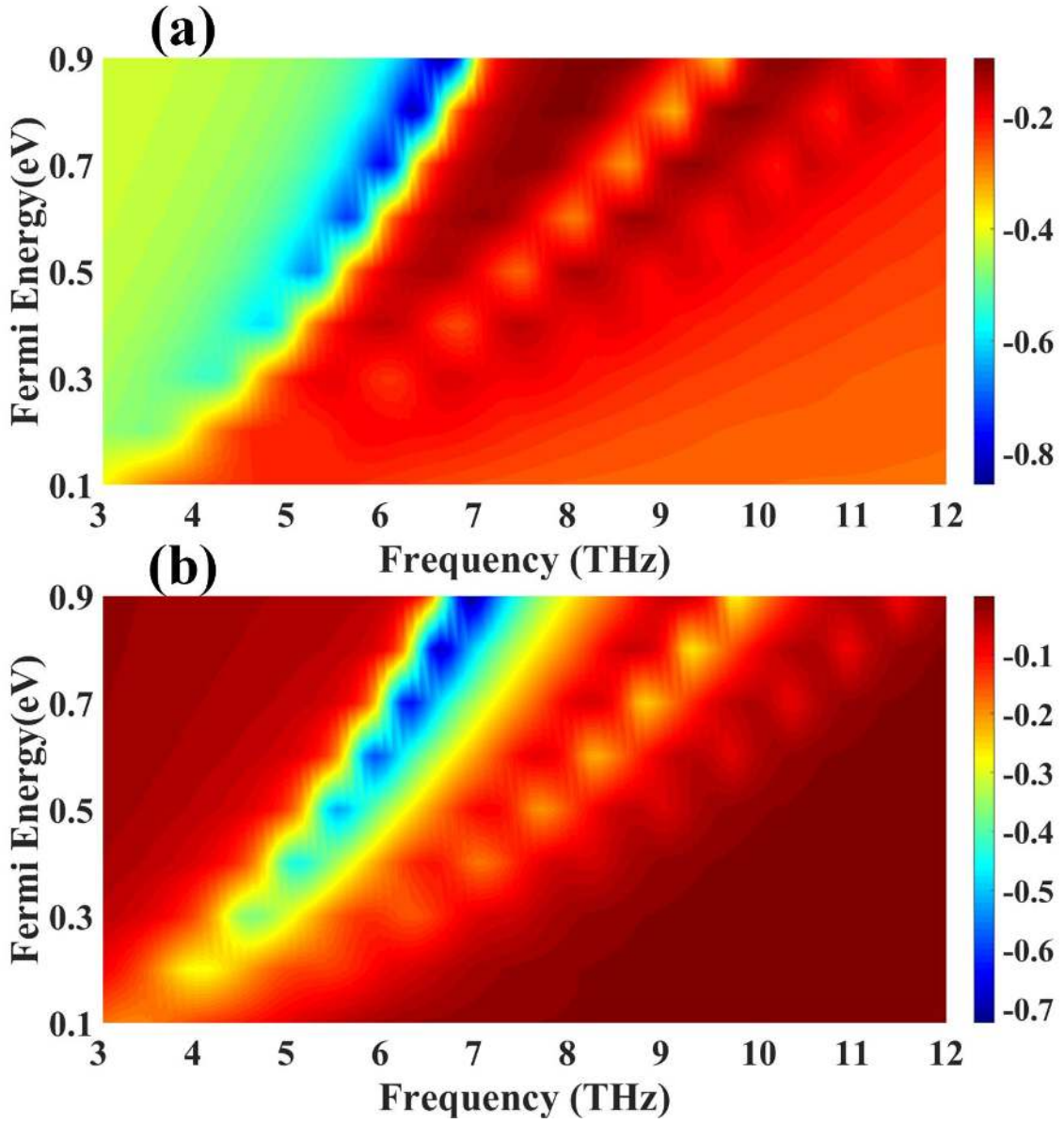

Fig 12: The effective refractive index for the X – polarized wave for the different values of Fermi energy and frequency. (a) real part response and (b) imaginary part response of the refractive index.

Effective refractive indices

The effective refractive indices of the proposed polarizer structure are calculated from the equation given in [32]. The metamaterial state of the proposed structure can be identified from Fig. 12 and Fig. 13. Fig. 12 shows the variation on the effective refractive index for the different Fermi energy values and frequencies. Fig. 12(a) and Fig.12(b) show the real and imaginary part of the effective refractive index for the X – polarized incident wave condition. Similarly, Fig. 13(a) and Fig. 13(b) show the variation in the real and imaginary values for the effective refractive index for the Y-polarized wave condition. It is observed that the negative values of the effective refractive index on both polarization modes, will ultimately prove the behavior of the polarizer as a metamaterial device. Values of the effective refractive index also change as the function of graphene Fermi energy and frequency as observed in Fig. 12 and Fig. 13.

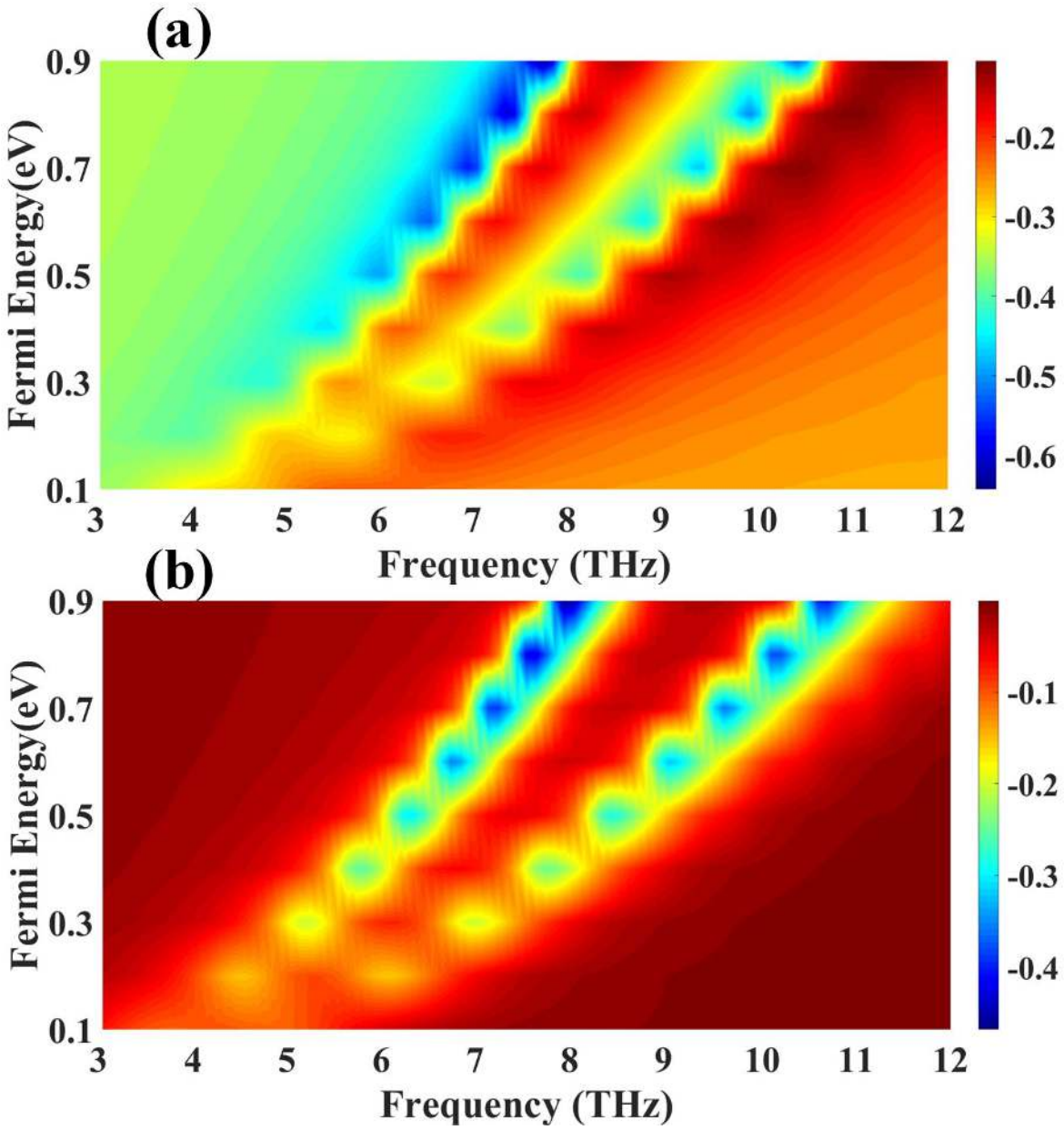

Fig 13: The effective refractive index for the Y – polarized wave for the different values of Fermi energy and frequency. (a) real part response and (b) imaginary part response of the refractive index.

Conclusion

In conclusion, the graphene-based tunable broadband polarizer is investigated over the far-infrared frequency range of 3 to 12 THz. The polarizer structure is investigated to identify the cross-polarization and co-polarization behavior for the different (X and Y) polarized input conditions. The proposed graphene-based polarizer is tunable for the different Fermi energy values of graphene. PCR values of the cross-polarization and co-polarization prove the behavior of the polarizer structure over a broad range of the frequency. The refractive indices values from reflectance and transmittance were also calculated to analyze the behavior as a metamaterial device. The proposed polarizer structure can be used in a broad range of the THz frequency due to the wide bandwidth of the reflectance response. The wide-angle incident behavior upto 60° of the input waves has been observed. The presented results can lead to new tunable THz devices for electro-optical structures operating in lower THz frequencies. The simple, compact and tunable design of the graphene-based polarizer structure is the capability to become the basic building block of large THz integrated systems.

Funding: There is no funding support for this research.

Conflicts of interest/Competing interests: The authors declare that they have no known competing financial interests or personal relationships that could have appeared to influence the work reported in this paper.

Availability of data and material: Raw data of the computed results were generated at Marwadi University. Derived data supporting the findings of this study are available from the corresponding author on request.

Code availability: Not applicable.

Authors' contributions: Vishal sorathiya conceive the project, simulated the proposed structure, generated the results, and contributed to writing the manuscript for this research. S K Patel supervises the overall project at every stage.

Ethics approval: All applicable international, national, and/or institutional guidelines for the care and use of animals were followed

Consent to participate: Not applicable

Consent for publication: Not applicable

References

[1] L. Qi and C. Liu, “Broadband multilayer graphene metamaterial absorbers,” *Opt. Mater. Express*, vol. 9, no. 3, p. 1298, 2019.

[2] V. Sorathiya, S. K. Patel, and D. Katrodiya, “Tunable graphene-silica hybrid metasurface for far-infrared frequency,” *Opt. Mater. (Amst).*, vol. 91, pp. 155–170, May 2019.

[3] Z. Song, K. Wang, J. Li, and Q. H. Liu, “Broadband tunable terahertz absorber based on vanadium dioxide metamaterials,” *Opt. Express*, vol. 26, no. 6, p. 7148, Mar. 2018.

[4] D. R. Smith, W. J. Padilla, D. C. Vier, S. C. Nemat-Nasser, and S. Schultz, “Composite medium with simultaneously negative permeability and permittivity,” *Phys. Rev. Lett.*, vol. 84, no. 18, pp. 4184–4187, May 2000.

[5] J. B. Pendry, “Negative Refraction Makes a Perfect Lens,” *Phys. Rev. Lett.*, vol. 85, no. 18, pp. 3966–3969, Oct. 2000.

[6] A. K. Geim and K. S. Novoselov, “The rise of graphene.,” *Nat. Mater.*, vol. 6, no. 3, pp. 183–91, Mar. 2007.

[7] M. Kaliberda, L. Lytvynenko, and S. Pogarsky, “Singular integral equations in diffraction by multilayer grating of graphene strips in the THz range,” *Eur. Phys. J. Appl. Phys.*, vol. 82, no. 2, p. 21301, 2018.

[8] V. Dave, V. Sorathiya, T. Guo, and S. K. Patel, “Graphene based tunable broadband far-infrared absorber,” *Superlattices Microstruct.*, vol. 124, pp. 113–120, Dec. 2018.

[9] H. Xiong, Y.-B. Wu, J. Dong, M.-C. Tang, Y.-N. Jiang, and X.-P. Zeng, “Ultra-thin and broadband tunable metamaterial graphene absorber,” *Opt. Express*, vol. 26, no. 2, pp. 1681–1688, 2018.

[10] S. K. Patel, V. Sorathiya, T. Guo, and C. Argyropoulos, “Graphene-based directive optical leaky wave antenna,” *Microw. Opt. Technol. Lett.*, vol. 61, no. 1, pp. 153–157, Jan. 2019.

[11] G. W. Hanson, “Dyadic green’s functions for an anisotropic, non-local model of biased graphene,” *IEEE Trans. Antennas Propag.*, vol. 56, no. 3, pp. 747–757, 2008.

[12] T. Stauber, N. M. R. Peres, and A. K. Geim, “Optical conductivity of graphene in the visible region of the spectrum,” *Phys. Rev. B - Condens. Matter Mater. Phys.*, vol. 78, no. 8, pp. 1–8, 2008.

[13] G. W. Hanson, “Dyadic Green’s functions and guided surface waves for a surface conductivity model of graphene,” *J. Appl. Phys.*, vol. 103, no. 6, 2008.

[14] J. Horng *et al.*, “Drude conductivity of Dirac fermions in graphene,” *Phys. Rev. B - Condens. Matter Mater. Phys.*, vol. 83, no. 16, p. 165113, Apr. 2011.

[15] Z. Q. Li *et al.*, “Dirac charge dynamics in graphene by infrared spectroscopy,” *Nat. Phys.*, vol. 4, no. 7, pp. 532–535, 2008.

[16] R. Panwar and J. R. Lee, “Progress in frequency selective surface-based smart electromagnetic structures: A critical review,” *Aerosp. Sci. Technol.*, vol. 66, pp. 216–234, Jul. 2017.

[17] V. Sorathiya and V. Dave, “Numerical study of a high negative refractive index based tunable metamaterial structure by graphene split ring resonator for far infrared frequency,” *Opt. Commun.*, vol. 456, no. June 2019, p. 124581, 2020.

[18] R. Mishra, A. Sahu, and R. Panwar, “Cascaded Graphene Frequency Selective Surface Integrated Tunable Broadband Terahertz Metamaterial Absorber,” *IEEE Photonics J.*, vol. 11, no. 2, 2019.

[19] N. Liu, X. Sheng, C. Zhang, and D. Guo, “Design of Frequency Selective Surface Structure With High Angular Stability for Radome Application,” *IEEE Antennas Wirel. Propag. Lett.*, vol. 17, no. 1, pp. 138–141, Jan. 2018.

[20] Y. Dong, P. Liu, D. Yu, G. Li, and L. Yang, “A Tunable Ultrabroadband Ultrathin Terahertz Absorber Using Graphene Stacks,” *IEEE Antennas Wirel. Propag. Lett.*, vol. 16, pp. 1115–1118, 2017.

[21] Q. Guo, Z. Li, J. Su, J. Song, and L. Y. Yang, “Active Frequency Selective Surface with Wide Reconfigurable Passband,” *IEEE Access*, vol. 7, pp. 38348–38355, 2019.

[22] Q. Zhou *et al.*, “Independently controllable dual-band terahertz metamaterial absorber exploiting graphene,” *J. Phys. D. Appl. Phys.*, vol. 52, no. 25, 2019.

[23] K. S. Novoselov *et al.*, “Two-dimensional atomic crystals,” *Proc. Natl. Acad. Sci.*, vol. 102, no. 30, pp. 10451–10453, Jul. 2005.

[24] N. Petrone *et al.*, “Chemical Vapor Deposition-Derived Graphene with Electrical Performance of Exfoliated Graphene,” *Nano Lett.*, vol. 12, no. 6, pp. 2751–2756, Jun. 2012.

[25] E. Moreau *et al.*, “Graphene growth by molecular beam epitaxy on the carbon-face of SiC,” *Appl. Phys. Lett.*, vol. 97, no. 24, p. 241907, Dec. 2010.

[26] T. Zou *et al.*, “High-speed femtosecond laser plasmonic lithography and reduction of graphene oxide for anisotropic photoresponse,” *Light Sci. Appl.*, vol. 9, no. 1, 2020.

[27] L. Song, L. Ci, W. Gao, and P. M. Ajayan, “Transfer Printing of Graphene Using Gold Film,” *ACS Nano*, vol. 3, no. 6, pp. 1353–1356, Jun. 2009.

[28] M. C. Sherrott *et al.*, “Experimental Demonstration of >230° Phase Modulation in Gate-Tunable Graphene–Gold Reconfigurable Mid-Infrared Metasurfaces,” *Nano Lett.*, vol. 17, no. 5, pp. 3027–3034, May 2017.

[29] H. Cheng, S. Chen, P. Yu, J. Li, L. Deng, and J. Tian, “Mid-infrared tunable optical polarization converter composed of asymmetric graphene nanocrosses,” *Opt. Lett.*, vol. 38, no. 9, p. 1567, May 2013.

[30] J. Ding *et al.*, “Mid-Infrared Tunable Dual-Frequency Cross Polarization Converters Using Graphene-Based L-Shaped Nanoslot Array,” *Plasmonics*, vol. 10, no. 2, pp. 351–356, Apr. 2015.

[31] J. Hao *et al.*, “Optical metamaterial for polarization control,” *Phys. Rev. A*, vol. 80, no. 2, p. 023807, Aug. 2009.

[32] D. R. Smith, S. Schultz, P. Markoš, and C. M. Soukoulis, “Determination of effective permittivity and permeability of metamaterials from reflection and transmission coefficients,” *Phys. Rev. B - Condens. Matter Mater. Phys.*, vol. 65, no. 19, pp. 1–5, Apr. 2002.